Localization of Visual Codes using Fuzzy Inference System

Péter Bodnár and László G. Nyúl
Department of Image Processing and Computer Graphics, University of Szeged, Szeged, Hungary

Keywords: QR Code, Object Detection, Pattern Recognition, Image Texture Analysis, Histogram.

Abstract: Usage of computer-readable visual codes is common in everyday life. The reading process of visual codes consists of two steps, localization and data decoding. This paper introduces a fast and robust method for localization of visual codes using Fuzzy Inference Systems based on simplistic, attentive features which can be optionally extended with cell histograms. Input image properties, assigned membership functions and efficiency of the system has been evaluated and discussed, showing FIS is a viable alternative for rapid QR code recognition in the image domain. The basic approach can be also used with lookup tables, that speeds up image cell evaluation and makes it ideal for embedded systems.

1 INTRODUCTION

Two-dimensional visual code formats are designed aiming automatic readability by computers and embedded systems. Image quality and acquisition techniques vary considerably and each application has its own requirements for detection speed and accuracy, making the task more complex.

The recognition process consists of two steps, localization and decoding. There already are works proposing various ways to automatically localize codes in images. A paper suggests localization of the locator patterns of QR codes using three scan-lines (Chu et al., 2011), however, this is sensitive to noise and camera shaking. Other works (Ohbuchi et al., 2004; Lin and Lin, 2013) involve mathematical morphology, which is very tolerant to noise and blur, but it can also be time-consuming, thus making real-time implementations more difficult on embedded systems. There is also a work using Haar-based classifier for the locator patterns of QR codes (Belussi and Hirata, 2011), which is fast and can have high precision with a well-chosen application setup and training database.

A QR code is attentive, which means it requires little human observation to identify. Since its features are observable on a higher level than the texture of its carrier material, they are easy to recognize by humans, but difficult to quantitatively define. Terms and operators of fuzzy logic are a viable option for QR code localization based on statements that include vagueness and uncertainty.

In this paper, we propose a Fuzzy Inference System (FIS) based on the most simplistic, attentive features of a QR coded, and test the proposed algorithm on other popular 2D code types. The described approach can be efficient with respect to computation time and storage, and most of the computed features can be approximated using only a subset of pixels, that allows fine-tuning of the application to be faster or more accurate. These properties can make FIS-based localization a preferred choice over other existing algorithms. After the code is located, there are reliable methods for correction of camera shaking and orientation (Chu et al., 2011), and correction of perspective distortion (Ohbuchi et al., 2004). Decoding is not discussed here, since after a successful localization step, retrieving the embedded data can be considered straightforward.

2 THE PROPOSED LOCALIZATION METHOD

Input image is uniformly divided into square blocks of equal size. Each block serves as an input to the FIS. Features are computed, and the FIS shows how likely a QR code part is present in the block. After all blocks are evaluated, a feature matrix is formed by the values given for each block (Fig. 1(b)). Finally, the matrix is evaluated and regions of interests are formed, that can be re-mapped to image space, thus giving bounding boxes to QR code candidates.

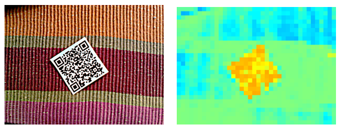

(a) (b)

Figure 1: Printed QR code on tablecloth (a) and its FIS feature image (b).

2.1 The Fuzzy Inference System

The proposed FIS consists of three input and one output variables. Membership function (MF) parameters are tuned each time to the end-user scenario using statistics of a few input images. For the selection of properties, we pursued simple features that represent humanly observable properties. The three properties can be summarized in the following statement: QR code parts consist of mostly black and white pixels of similar amounts, while having moderate to high contrast and low saturation.

2.1.1 Variables and Membership Functions

Our first variable is based on the absolute difference of pixels from the 50 % gray value. Intensity values referred in this paper, are normalized to $[0,1]$ from the 8-bit grayscale input images to fit the ranges of the membership functions. The first property is

$$\text{graydist\_avg} = \frac{1}{n}\sum_{p\in\text{block}} |V(p) - 0.5| \qquad (1)$$

where n denotes the number of sampled pixels from the block, and $V(p)$ is the V value of the pixel in HSV color space. From a couple of sample images, blocks being fully covered with QR code parts as positive samples, and blocks with 0 % coverage ratio as negatives, are extracted. After that, mean and standard deviation are computed for *graydist_avg*. This was 0.41 ± 0.04 for positive samples and 0.31 ± 0.12 for negatives in our first test set. That would define two Gaussian membership functions, *perfect*$(m = 0.41, \sigma = 0.04)$ and *low*$(m = 0.31, \sigma = 0.12)$, however, using those would let very small tolerance and they would not cover the whole input range. To overcome this, Z-shaped and S-shaped membership functions are used instead of Gaussians (Fig. 2(a)). A reasonable Z-term for *low* is $\text{ZMF}(0, 0.41)$, because the mean of *graydist_avg* was at 0.41. For *perfect*, an S-term of $\text{SMF}(0.31, 0.41)$ is proposed, since negative sample mean was 0.31, which means, from that point, we have no information about the block content according to this property. The endpoint of the S-term should be 0.41, since that was our measured mean value for the test images. This parameter would be 0.5 in the perfect case, and lower values reflect the amount of blurring present in blocks containing QR code parts.

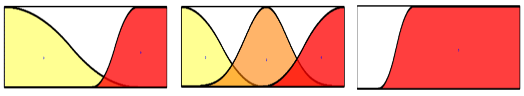

(a) (b) (c)

Figure 2: FIS input variables. (a): Mean brightness absolute difference from gray: *low* (yellow) and *perfect* (red); (b): Mean brightness: *low* (yellow), *perfect* (orange) and *high* (red); (c): Mean saturation: *high* (red). Parameters are indicated in the text.

The second input variable is *blockavg*, the mean intensity of the block. We obtained 0.52 ± 0.13 for positive, and 0.44 ± 0.31 for negative examples. Having this value around 0.5 for positive samples is expected because of the structure of the QR code. For negative samples, it is dependent on the content of the block. This property seems to have small classification power, however, having the value around 0.5 is a necessary condition for a positive sample. Three membership functions are proposed, one Gaussian for *perfect*$(m = 0.52, \sigma = 0.13)$ values, a $\text{ZMF}(0, 0.5)$ and a $\text{SMF}(0.5, 1)$ for *low* and *high* blocks, respectively (Fig. 2(b)). Both of the last two MFs express low certainty of presence of a QR code part within the block.

The third input parameter *saturation* excludes regions that have high saturation, since highly saturated areas are less likely to contain QR codes. The goal with saturation was to improve precision while keeping the hit rate. Mean saturation was 0.13 ± 0.05 for positive, and 0.39 ± 0.22 for negative samples, so a $\text{ZMF}(0.13, 0.39)$ is proposed as *high*, shown in Fig. 2(c).

The output of the FIS is *codeness*, the certainty of QR code texture within a block, which can be expressed by two MFs, $\text{ZMF}(0, 1 - x)$ and $\text{SMF}(x, 1)$ with $x \in [0, 0.5]$, providing different level of smooth transitions. We used an intermediate $x = 0.33$ value in our model, thus producing $\text{ZMF}(0, 0.67)$ and $\text{SMF}(0.33, 1)$ for *low* and *high* MFs, respecively.

2.1.2 Rules

The rule set of the FIS contains the following rules:

R1 **if** *blockavg* **is** *perfect* **and** *graydist_avg* **is** *perfect* **then** *codeness* **is** *high*

R2 **if** *blockavg* **is** *low* **or** *blockavg* **is** *high* **then** *codeness* **is** *low*

R3 **if** *graydist_avg* **is** *low* **then** *codeness* **is** *low*

R4 **if** *saturation* **is** *high* **then** *codeness* **is** *low*

R1 is about positive response. Having the *block-avg* and *graydist_avg* properties in range are required conditions that have to be met simultaneously. The *blockavg* is needed so *high codeness* cannot be achieved with solid black or solid white blocks which both have *low saturation* and *high graydist_avg*. Following the same logic, we assume some contrast within blocks, expressed by *graydist_avg*, so solid gray blocks will not result in *high codeness*. R2 is to connect *low* and *high* MFs of *blockavg*, since both indicate QR code part is not likely in that block. R3 filters out blocks by *graydist_avg* in a similar manner than the previous one. R4 is another exclusion filter, which is based on the mean of saturation, as discussed above.

2.1.3 Operators

For conjunction, *minimum* and a couple of product operators are available, which behave similarly, and show no significant difference in our case. *Minimum* operator is the simplest to compute. Both *blockavg* and *graydist_avg* has to be high for *high codeness*, and the decision based on the minimum of these variables suits our model. Products, like *algebraic product* can also be used, however, they lead to a stricter rule and steeper decision surface. For disjunction operator, the *maximum* is recommended with this rule set and MF layout, since that is the simplest operator to compute, and in this case, where no overlapping is present between the MFs participating in the conjunction (Fig. 2), there is no difference in the results of *maximum* and the various *x-sum* operators available. For the case of simplicity, *minimum* can be used for activation. The usage of *algebraic product* would result in smoother transitions with the defuzzified output variable, however, it does not affect accuracy of the FIS significantly. For accumulation operator, the *maximum* is recommended, since there are only two MFs of the output, and they are also symmetrically situated, thus there is no need to use complex operators at that step. In the defuzzification step, we used *Centroid*, since it provides smooth transition of the output.

2.2 Feature Matrix and Regions of Interest

A simple approach to process the matrix is binarization by a threshold, followed by connected component labeling, further filtered by size and compactness. Calculation of the summed area matrix can further increase processing speed.

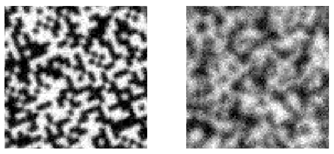

(a) QR-50 (b) QR-100

Figure 3: Enlarged QR code parts with different amounts of noise present.

2.3 Extension of the Feature Set with Cell Histogram

While the above features are obtained from pixel data, they can also be considered as a simplification of the histogram. In some cases, the histogram is also useful in the formation of a new input property for the FIS, when the above inputs are not sufficient.

In case of an ideal cell containing a part of a QR code, only black and white intensities are present cell-wise in roughly 1:1 proportion. Smoothing of images that contain QR code, introduces intensities closer to the mean, and decreases the value of extreme histogram bins, like the ones belonging to black and white. In general, the peaks are lowered, some bins close to the peaks receive higher values, and others keep their values. As a very simplistic approach, a constant (C) can be added to the expected density function. The proposed value of C can be the estimated proportion of the smoothing kernel width (3 times its σ) and the code element width. As the Gaussian kernel width increases, the code element contrast gets lower, and at some point, code elements become unreadable. This roughly happens when the kernel size exceeds the code element size. Considering this, the maximum Gaussian kernels used in our synthetic test set has the same width as the undistorted code element. Noise is also added to the model with Gaussian distribution, having σ in the [0, 0.25] range in the test database. Fig. 3(b) shows that these amounts of noise and blur theoretically destroy the value of a code element. The value x in QR-x denote the percentage of noise and blur added, up to these discussed maxima (QR-0 and QR-100 are the perfect and the hardest cases of the data set, respectively).

The proper values of σ and C can be approximated empirically by showing test images to the camera, with solid cells of bright and dark intensities, and with lines of different thickness.

Considering the amount of noise and blur this way, the desired histogram to a particular camera setup can be expressed in the $[0,1]$ interval as

$$U_{C,\sigma}(x) = C + (1-C)\left(e^{-\frac{x^2}{(\varepsilon+\sigma)^2}} + e^{-\frac{(1-x)^2}{(\varepsilon+\sigma)^2}}\right), \quad (2)$$

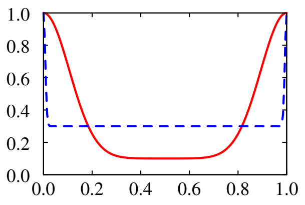

Figure 4: Expected probability functions. Red solid curve: small C (expected smoothing) with moderate amount of expected noise $C = 0.1$, $\sigma = 0.15$ (example for dirty environment), blue dashed curve: larger C with smaller amount of expected noise $C = 0.3$, $\sigma = 0.01$ (example for low quality phone camera).

where ε denotes a small positive value to prevent division by zero in the perfect case. After sampling the function and normalization of the data, a desired distribution is obtained. Different values of σ and C lead to different distributions (Fig. 4). For cameras having low dynamic range, contrast stretching is recommended as a pre-processing step.

Histograms are more reliable when based on more pixels, however, our goal using the least number of pixels possible. To overcome inaccuracies that come from histograms based on a small amount of pixels, histogram binning is recommended.

With a given number of histogram bins b we can compute the dissimilarity of the desired and measured histograms using various well-known formulas. Let $B(i)$ the number of pixels that fall into the i-th intensity bin in the measured cell histogram, $B_n(i)$ the normalized $B(i)$ and $U_n(i)$ the binned, normalized U-function

$$U_n(i) = \frac{\int_{i/b}^{(i+1)/b} U_{C,\sigma}(x)}{\int_0^1 U_{C,\sigma}(x)}. \qquad (3)$$

For simplicity, we omit the parameters C and σ from the notation of binned, normalized U-function and from the derived distance measures. Nevertheless, for any choice of parameters C and σ, there exist a distance measure of the types defined below. Eucledian distance can be given as

$$D_e(B_n, U_n) = \frac{1}{2}\sqrt{\sum_{i=1}^{b}(B_n(i) - U_n(i))^2}, \qquad (4)$$

however, that is a bin-by-bin dissimilarity measure, which is sensitive to noise and the number of bins (Swain and Ballard, 1991).

Normalized histograms can also be considered as probability density functions. A common way to compare those is the Kolmogorov-Smirnov distance

$$D_k(B_n, U_n) = \max_i(|\hat{B}_n(i) - \hat{U}_n(i)|), \qquad (5)$$

Table 1: Eucledian, Kolmogorov-Smirnov and EMD similarity of measured histograms to the ideal histograms, using QR code pieces of different quality.

S_e	QR-0	QR-50	QR-100	Flat	Black
$U_{0,0}$	1.000	0.7653	0.6495	0.6938	0.6464
$U_{0.12,0.12}$	0.8381	0.9210	0.7950	0.8510	0.6111
$U_{0.25,0.25}$	0.7531	0.9587	0.8543	0.9243	0.5687
S_k	QR-0	QR-50	QR-100	Flat	Black
$U_{0,0}$	1.000	0.6739	0.5416	0.6250	0.5000
$U_{0.12,0.12}$	0.8045	0.8694	0.7196	0.8205	0.3045
$U_{0.25,0.25}$	0.7020	0.9327	0.7725	0.9024	0.2020
S_m	QR-0	QR-50	QR-100	Flat	Black
$U_{0,0}$	1.000	0.8599	0.7522	0.8125	0.5625
$U_{0.12,0.12}$	0.9140	0.9431	0.8382	0.8985	0.5625
$U_{0.25,0.25}$	0.8716	0.9610	0.8806	0.9409	0.5625

where $\hat{B}_n(i)$ and $\hat{U}_n(i)$ are cumulative histograms for the first i elements. This distance measure is widely used for cross-bin comparison of color histograms. Rubner et al. (Rubner et al., 2000) also proposes earth mover's distance (EMD) for comparison for multichannel images, and normalized matching distance

$$D_m(B_n, U_n) = \frac{1}{b}\sum_{i}^{b}|\hat{B}_n(i) - \hat{U}_n(i)| \qquad (6)$$

as a special case, which is suitable for grayscale histograms.

Table 1 shows values of these similarity values ($S_X = 1 - D_X | X \in \{e, k, m\}$) for desired distributions $U_{0,0}$, $U_{0.12,0.12}$ and $U_{0.25,0.25}$, compared to synthetic QR codes of different levels of quality (Fig. 3), a flat histogram $F(x) = 1/b$, and histogram of a solid black image. We recommend using the matching distance D_m for histogram comparison, since it shows significantly higher values for this feature in the positive case.

Results show that cell histograms of the hardest images of the set (QR-100) have cell histograms that show very small resemblance to the histogram of our model. This is due to noise, smoothing, and histogram asymmetry caused by the visual pattern variability of the embedded data.

2.3.1 Patterns and Cell Size

Not all pixels are necessary to be sampled from the cell, we can approximate the histogram using only a subset of the pixels. This is sufficient for images having only small amount of imperfections and noise, while it reduces the computation time. However, if the variance of QR code size is large, this undersampling is quite risky because depending on the size of the code elements in the image, the proposed method might miss so many elements that the histogram looks very different from a typical QR code histogram.

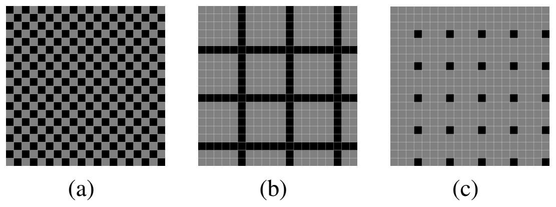

Figure 5: Cell patterns for histogram sampling. (a) checkerboard pattern using 50 %, (b) 5:1 linear pattern using cca. 36 %, and (c) sparse pattern using 6.25 % of pixels for each cell.

We recommend uniform sampling of the cell. The checkerboard pattern is a good option, and the amount of pixels can be further reduced using other patterns (Fig. 5).

Cell size should be small enough to having many of them to build a QR code, so threshold would be chosen easily for dropping or keeping cell groups. On the other hand, it has to be large enough to provide reliable statistical data for the histogram, at least tens of pixels for each bin. Papers on visual code localization suggest empirically (Bodnár and Nyúl, 2012), or using geometrical approach (Bodnár and Nyúl, 2013), that optimal tile size is about $1/3$ of the smaller dimension of the expected visual code in case of features based on image partitioning. The number of histogram bins can also be tuned to fulfill reliability and robustness. Too many histogram bins leads to sensitivity to noise, while choosing too few bins result in losing the feature. We recommend about 8 to 16 bins for 8-bit grayscale images. The range of expected code size, the desired number of bins and the mean pixel count falling into each bin determines the usable pattern and block size for detection. From another point of view, the number of bins, the expected mean pixel count and the block coverage ratio of the chosen pattern defines the size of the smallest detectable visual code.

3 EVALUATION AND RESULTS

The proposed method has been evaluated on 98 arbitrarily acquired images using a 3.2 Mpx Huawei smartphone camera, without auto-focus capabilities and flash. Unit size of the QR codes present in those images were about 6–10 pixels, overall QR code size was cca. 200×200 pixels. Image size was 800×600 pixels. An example from this set is shown on Fig. 1. Even lighting is preferred, but not necessary for the captured images. Images with uneven lighting has to be pre-processed with local contrast stretching performed in each block. Color images are also preferred for the saturation rule, that can be replaced by the rule based on histograms in case of grayscale input images. Geometrical distortions of the code leave the above features intact, as long as there are sufficient blocks to form a ROI in the feature matrix.

A Core 2 Duo 3.00 GHz CPU could process roughly 20 of these images each second, so real-time localization is possible. The FIS can be further optimized using ramp terms instead of ZMF and SMF. HSV channel images can be easily computed from RGB channels using $V_i = \max(R_i, G_i, B_i)$ and $S_i = (\max(R_i, G_i, B_i) - \min(R_i, G_i, B_i))/V_i$ for all $i \in I(x,y)$. Furthermore, using a lookup table instead of online calculations is also possible, since the table only would take one megabyte of data using precision of two decimals, which is sufficient for the task.

Table 2: Evaluation of the FIS on different block offsets and 40 px block size.

Block offset	T_{opt}	F-score	Precision	Hit rate	AUC
10 px	0.62	0.8124	0.8349	0.8766	0.8934
20 px	0.62	0.8124	0.8354	0.8773	0.8938
40 px	0.62	0.8584	0.8377	0.8802	0.8709

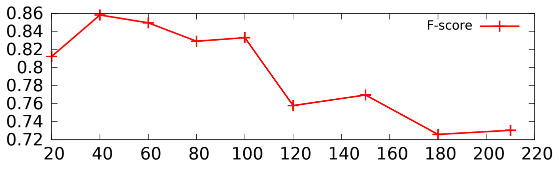

Figure 6: Performance of the FIS with respect to block size.

As the first test, various block sizes were evaluated to determine optimal block size ratio according to the expected QR code size, not involving histograms. Results show that optimal block size is ranging from about 20 to 35 percent of the QR code size (Fig. 6). Performance measures were based on the Jaccard measure. Choosing too small block size leads to performance drop, since the attributes computed from the blocks become less reliable, while too large block sizes also decrease accuracy, since then only a smaller number of blocks are fully covered with a QR code part, and partially covered blocks are also harder to classify. Instead of a fully universal, multi-scale solution (Lindeberg, 1993), specific resolutions and block sizes lead to more accurate implementations that can be important on embedded systems.

The effect of the block overlap to performance was also evaluated and is shown in Table 2. Block size was set to 40 px and each block was offset by 10, 20 and 40 px (meaning no overlap), respectively. Results show that evaluation with overlapping blocks did not increase performance.

Performance of the FIS has also been evaluated on code types other than QR codes. We assem-

Table 3: FIS performance on different visual code types. 1D-S denote for stacked barcodes.

Type	Dim.	Block size	Precision	Hit rate	F-score
QR	2D	50 px	0.9224	0.9353	0.9288
Aztec	2D	50 px	0.8738	0.9639	0.9167
Data matrix	2D	50 px	0.9214	0.9399	0.9305
Codablock	1D-S	20 px	0.7136	0.7287	0.7210
PDF417	1D-S	20 px	0.7277	0.7007	0.7140

bled four test sets containing Aztec codes and Data matrix codes as two-dimensional, and Codablock and PDF417 codes as stacked one-dimensional types. Stacked 1D codes, like real 2D ones, embed information along both axes. These synthetic examples are built with computer-generated codes containing random letters and numerals of the alphabet. The code was placed on a negative image, with random rotation. Gaussian smoothing and noise have been gradually added to the images. The σ for the Gaussian kernel was varied in the range [0,3]. A noise image (I_n) was generated with intensities ranging from [-127, 127] following normal distribution, and added gradually to the original 8-bit image (I_o) as $I = \alpha I_n + (1-\alpha)I_o$, with α ranging [0, 0.5]. The noise was added to the image using saturation arithmetic.

Results show that real 2D codes behave similarly to QR codes, despite their structural differences (Table 3). One-dimensional stacked codes had smaller height, therefore the block size has been set to smaller, however, localization performance was inferior to that for real 2D codes. This is probably due to the fact that in real 2D codes row and column patterns are similar while in stacked 1D codes they are quite different. The input variables used for the FIS are basically direction-invariant and thus suit better for 2D codes.

To compare efficiency of the proposed method to other implementations from the state of the art, we evaluated it on two public databases, from Sörös et al. (Sörös and Flörkemeier, 2013), and Dubská et al. (Dubská et al., 2013), respectively.

Sörös et al. made their set using 200 blurry images acquired by iPhone5, without auto-focus. The evaluation of the FIS on this set was performed with minor modifications of the original input terms based on sample images of the set. The *graydist_avg* attribute had its *perfect* SMF term adjusted to $\mathrm{SMF}(0.25, 0.5)$, since images of this set had poor contrast due to the heavy blur present. Mean intensity of the blocks were also higher, so the Gaussian term representing the *perfect* membership function has been modified to $G(m = 0.61, \sigma = 0.09)$. SMF term regarding saturation could be set to $\mathrm{SMF}(0.075, 0.19)$, which led to a stricter saturation rule than the one of our original test set. Results in Table 4 show performance of the

Table 4: Results of the proposed method on the Sörös et al. and Dubská et al. data sets.

Data set	Precision	Hit rate	F-score
Sörös et al. (Original FIS)	0.5938	0.5224	0.5558
Sörös et al. (Median filtered)	0.5890	0.6018	0.5953
Dubská et al. Set-1	0.6165	0.5036	0.5544
Dubská et al. Set-2	0.9288	0.9513	0.9399

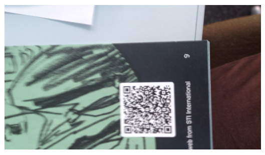
(a)

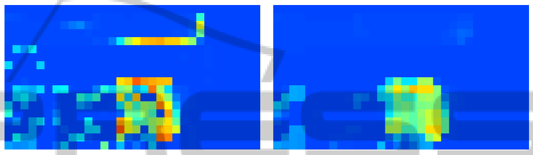
(b) (c)

Figure 7: Output stabilization of a sample image from the Sörös et al. set. (a) original image, (b) feature image, (c) median filtered feature matrix.

FIS on this test set for the original algorithm, and one with median filter as post-processing. Fig. 7 shows an example of this data set with the corresponding feature images.

The second public database by Dubská et al. contained two similar sets of QR code images, surrounded with text in a scene having low saturation in general. The first set has 410 high-resolution (2560×1440 px) images with uneven lighting conditions, high grades of distortion and minor blur (Fig. 8(a)). The second test set has 400 low-resolution (604×402 px) images with smaller grades of distortion and more even illumination, but having less light in general, thus producing darker images (Fig. 8(c)). For the first set of this database, FIS had to be set for larger tolerances for the *perfect* term of *blockavg*, and *graydist_avg* was also set to lower acceptance value, defined by $\mathrm{SMF}(0.25, 0.3)$. However, images of the first set have shown so high variability for the mean intensities within blocks, contrast and QR code size that the designed FIS could not be generalized enough to classify all samples well. We can overcome this issue using adaptive thresholding or local contrast stretching, at the cost of more computation time. On the second data set, with a chosen block size 50 px, FIS terms of positive response could be tuned more easily, therefore the proposed method performed better with respect to both precition and hit rate (Table 4).

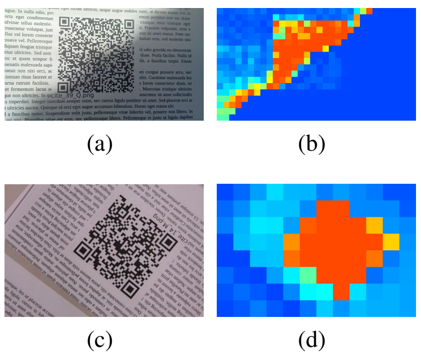

Figure 8: Examples of the Dubská et al. Set-1 (a) and Set-2 (c), and their feature images (b) and (d), respectively. In both cases the block size was 60 px, but the size of the first image is much higher than that of the second.

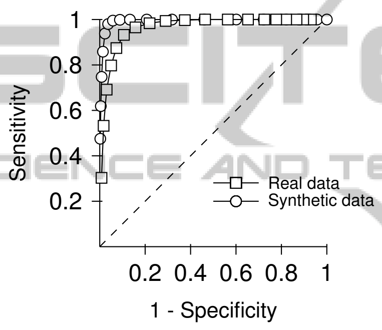

Figure 9: Efficiency of the proposed algorithm according to different thresholds, visualized in ROC space.

3.1 Performance Measures of the Cell Histogram Feature

Four variants of the histogram-based feature was evaluated separately from the FIS, each named after the pattern they use for building the cell histograms (HIST-FULL uses all pixels, HIST-CHK, HIST-LIN and HIST-SPA uses the checkerboard, linear and sparse patterns, respectively), and compared to the works of Ohbuchi et al. (Ohbuchi et al., 2004) and Lin et al. (Lin and Lin, 2013).

The effect of chosen threshold T to efficiency, using HIST-FULL, is shown in Fig. 9. AUC for synthetic and real data are 0.9924 and 0.8938, respectively. Sensitivity drops below 1.0 at $T = 0.73$, and F-measure peaks at $T = 0.86$. For industrial setups, where localization of all codes is crucial, we recommend $T \approx 0.8$, since sensitivity is still 99 % and precision is about 50 %. The behavior for chosen threshold and noise level is similar in all chosen patterns. Fig. 10 shows that noise has no significant effect to false positive rate, it only drops sensitivity at higher rates. Detailed results are shown in Table 5 for synthetic and real images of the database.

Table 5: Performance measures of the proposed algorithm using different cell patterns, compared to other localization approaches (Ohbuchi et al., 2004; Lin and Lin, 2013).

Synthetic images	Precision	Recall	Accuracy
REF-OHBUCHI	1.0000	0.837	0.8730
REF-LIN	0.9340	0.9490	0.8890
HIST-FULL	0.8320	0.9382	0.9732
HIST-CHK	0.8576	0.9035	0.9737
HIST-LIN	0.6625	0.9389	0.9426
HIST-SPA	0.6729	0.9014	0.9429
Real images	**Precision**	**Recall**	**Accuracy**
REF-OHBUCHI	0.9500	0.8750	0.8360
REF-LIN	0.9400	0.8930	0.8450
HIST-FULL	0.7672	0.9011	0.9630
HIST-CHK	0.7677	0.9016	0.9631
HIST-LIN	0.7662	0.9056	0.9632
HIST-SPA	0.7652	0.9005	0.9627

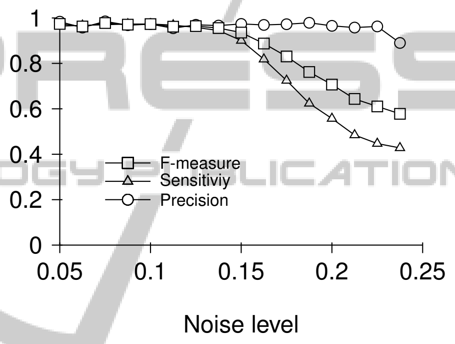

Figure 10: Precision, Sensitivity and F-measure according to noise level, using 0.86 as threshold.

3.2 Using Partial Block Information

As in the case of histograms, the number of read pixels can be limited to speed up FIS processing. Fig. 11 shows results of the sparse data evaluation. The x axis represents the sampling factor, which means that only every n-th pixel is read from both the rows and columns, so the amount of pixels used to calculate the FIS input variables, is reduced by a factor of n^2. This partial block information does not introduce more false positives, it only affects the hit rate by rendering the only rule of positive response unreliable in the FIS. Results also show that the chosen sampling interferes with the unit size of the QR code. Hit rate temporally rises while reading only every 10th, 12th and 15th pixel, since it gives a more reliable block sampling for attribute computation, which is caused by the cca. 6 px unit size of the used QR codes in those images. Choosing the sampling factor $k \cdot \text{unitsize}/2, (k \in \mathbb{Z})$ is more likely to sample most QR code units from the same position, like close to center of unit, or close to their perimeter. However, we cannot make any assumptions on expected QR unit size on arbitrarily acquired images, therefore us-

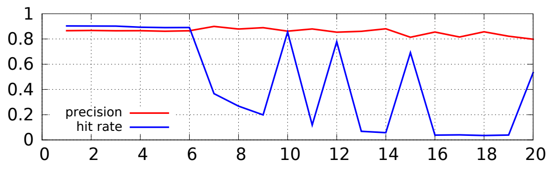

Figure 11: Performance of the FIS on sparse data. Values of the x axis mean that only every n-th pixel is read with respect to rows and columns.

ing large sampling factor is considered unreliable in general. Furthermore, chosen block size gives an upper limit to sampling, since calculation of the FIS input attributes are based on statistics and therefore require tens of pixels for each block. In order to stabilize the FIS output by region compactness, we could take adjacent blocks into consideration. To avoid large increase of computation time, evaluation of this condition is recommended to be performed outside the FIS, in the feature matrix. Small "holes" of the matrix, values surrounded by blocks of high values, are likely to be false negatives. Similarly, "lonely" blocks of high value can be safely zeroed out, since they probably do not participate in any QR code candidate. Morphological filtering, or as a simpler operation, median filtering are suitable for this task (Fig. 7). In most cases, the latter seems sufficient according to experimental results, however, using morphology at this step is also acceptable, since the size of the feature matrix is only a small fraction of that of the original input image.

4 CONCLUDING REMARKS

In this paper, we have shown that Fuzzy Inference Systems can be used to rapidly localize QR codes in the image domain. We have examined efficiency of Fuzzy Inference Systems that has membership functions created by preliminary assumptions based on statistics of a few sample images of the expected scenario. For industrial setups, making this assumption is easy, since variability of the content is smaller. For smartphone applications, parameters can be tuned using camera properties. Performance has been evaluated on public test image sets.

Block size and amount of overlap has also been evaluated, thus giving information about the robustness of the approach. FIS can be replaced by lookup tables that leads to constant-time evaluation. Calculation of the input features can be further accelerated using approximations with only a subset of intensity values. These properties can make FIS-based localization a preferred choice over other algorithms.

The proposed algorithm can also be used to efficiently localize other popular two-dimensional code types as well, like Aztec codes or Data matrix codes, without major modification.

ACKNOWLEDGEMENT

This publication is supported by the European Union and co-funded by the European Social Fund. Project title: Telemedicine-oriented research activities in the fields of mathematics, informatics and medical sciences. Project number: TÁMOP-4.2.2.A-11/1/KONV-2012-0073.

REFERENCES

Belussi, L. F. F. and Hirata, N. S. T. (2011). Fast QR code detection in arbitrarily acquired images. In *Graphics, Patterns and Images (Sibgrapi), 2011 24th SIBGRAPI Conference on*, pages 281–288.

Bodnár, P. and Nyúl, L. G. (2012). Improving barcode detection with combination of simple detectors. In *The 8th International Conference on Signal Image Technology (SITIS 2012)*, pages 300–306.

Bodnár, P. and Nyúl, L. G. (2013). A novel method for barcode localization in image domain. In *Image Analysis and Recognition*, volume 7950 of *Lecture Notes in Computer Science*, pages 189–196.

Chu, C.-H., Yang, D.-N., Pan, Y.-L., and Chen, M.-S. (2011). Stabilization and extraction of 2D barcodes for camera phones. *Multimedia Systems*, 17:113–133.

Dubská, M., Herout, A., and Havel, J. (2013). Real-time precise detection of regular grids and matrix codes. *Journal of Real-Time Image Processing*, pages 1–8.

Lin, D.-T. and Lin, C.-L. (2013). Automatic location for multi-symbology and multiple 1D and 2D barcodes. *Journal of Marine Science and Technology*, 21(6):663–668.

Lindeberg, T. (1993). *Scale-space theory in computer vision*. Springer.

Ohbuchi, E., Hanaizumi, H., and Hock, L. A. (2004). Barcode readers using the camera device in mobile phones. In *Cyberworlds, 2004 International Conference on*, pages 260–265.

Rubner, Y., Tomasi, C., and Guibas, L. J. (2000). The earth mover's distance as a metric for image retrieval. *International Journal of Computer Vision*, 40(2):99–121.

Sörös, G. and Flörkemeier, C. (2013). Blur-resistant joint 1D and 2D barcode localization for smartphones. In *Proceedings of the 12th International Conference on Mobile and Ubiquitous Multimedia*, MUM '13, pages 11:1–11:8, New York, NY, USA. ACM.

Swain, M. J. and Ballard, D. H. (1991). Color indexing. *Int. J. Comput. Vision*, 7(1):11–32.